International Journal of Emerging Trends & Technology in Computer Science (IJETTCS)
Web Site: www.ijettcs.org Email: editor@ijettcs.org
Volume 6, Issue 6, November- December 2017 ISSN 2278-6856

Wireless Power Transfer (WPT) systems for charging consumer devices

SUJAY RAVI KALE[1], K.Chandra obula reddy[2]

[1]Student (M.E) Electrical Engineering Department, MSS's COE, BAMU university, Jalna, Maharastra-431203

[2]Asst.professor, Electrical Engineering Department, MSS's COE, BAMU university, Jalna, Maharastra-431203

Abstract

Wireless power transfer (WPT) is an emerging technology with an increasing number of potential applications totransfer power from a transmitter to a mobile receiver over a relatively large air gap. However, its widespread application is hampereddue to the relatively low efficiency of currentWireless power transfer (WPT) systems. This study presents a concept to maximizethe efficiency as well as to increase the amount of extractable power of a WPT system operating in non resonant operation. Theproposed method is based on actively modifying the equivalent secondary-side load impedance by controlling the phase-shift ofthe active rectifier and its output voltage level. The presented hardware prototype represents a complete wireless charging system,including a dc–dc converter which is used to charge a battery at the output of the system. Experimental results are shown for theproposed concept in comparison to a conventional synchronous rectification approach. The presented optimization method clearlyoutperforms state-of-the-art solutions in terms of efficiency and extractable power.

Keywords: Dc-dc power converters, impedancematching, inductive power transmission, phase-shift control, reactive powercontrol, rectifiers, wireless charging.

1. INTRODUCTION

WIRELESS power transfer (WPT) is used in various application fields ranging from a few milli watts in biomedical applications [1]–[3] up to several kilowatts of output power in automotive applications [4]–[6]. Currently, WPT systems intended to wirelessly charge consumer electronic devices, such as mobile phones or tablet computers, are studied extensively [7]. Various aspects of these systems are defined by several standards which are either based on non resonant or inductive power transfer (IPT), like the Qi standard [11] or on resonant power transfer (RPT), like the Rezence standard. In order to ensure interoperability of different transmitter and receiver devices, these standards define parameters such as the voltage range, the basic circuit structure, and the operating frequency of the system. The main drawbacks of currently available WPT systems for consumer applications are, amongst others, the relatively low overall efficiency and the limited power transfer capability. This results in long charging times which hampers the widespread application of the WPT technology. To overcome these problems, various improvements have been suggested in the literature. Design and optimization methodologies for increasing the efficiency or the maximum transferable power of a WPT link have been proposed in [13]–[16], assuming that the system parameters are freely selectable. However, these optimization strategies are not applicable to commercial charging applications, where the system parameters are defined by a standard. On the other hand, various optimization methods which are in accordance with current standards are reported. In, different control strategies for the transmitter of a WPT system are compared regarding their impact on the output power and the efficiency. Furthermore, in, a control scheme for a synchronous rectifier on the secondary side is proposed to improve the efficiency in comparison to a passive and semi active rectifier solution.

Although WPT has been extensively studied in recent years ,less attention has been paid to the optimization of an entire wireless charging system, starting from a dc input source to charging a battery at the output. In, a Qi compliant wireless charging system has been presented but only commercial available components have been used and no advanced optimization techniques have been applied to increase the system efficiency and the extractable output power. In [9], a dual mode receiver architecture is presented which is capable of operating according to the Qi standard (110–205 kHz) and the Rezence standard (6.78 MHz). Experimental results, from the input of the rectifier to the battery at the output, show a higher efficiency for the nonresonant operating mode mainly due to lower switching losses. In a wireless charging system the efficiency and the amount of power transferred to the output are influenced by the source (transmitter) and load (receiver) impedances. In, the load impedance is assumed to be purely resistive and, therefore, efficiency improvements are reported by only adjusting the resistive part of the load impedance. However, this approach does not yield optimal efficiency for the whole operating range, since only the resistive part of the load impedance is altered and the reactive part is not considered at all. The maximum amount of power can be transferred by modifying the load impedance to match the complex conjugate of the source impedance. An impedance adjustment unit is applied in to cancel the reactive part of the impedance and thereafter to alter the resistive part in order to yield maximum power transfer. Yet, this technique uses a network of passive components to adjust the impedance, and it targets only to achieve the maximum extractable output power while the system efficiency is not optimized. Additional improvements to the efficiency of a

WPT system are obtained by actively modifying the reactive part of the load impedance. In , a phase-shift control approach, instead of a conventional controlling method, is applied to the active rectifier on the secondary side of an RPT system. This technique is used to achieve efficiency improvements by modifying the secondary side resonance frequency, but on the other hand it also impacts the equivalent load impedance. Since the phase-shift is the only control parameter, the resistive as well as the reactive part of the equivalent load impedance are concurrently altered. Hence, these two parameters cannot be controlled separately and the point of maximum efficiency is not reached in general. Furthermore, it might be highlighted that solely investigates an RPT system with a resistive load at the output of the rectifier. In this study, an advanced optimization strategy for an entire wireless charging system, including an active rectifier and a dc–dc converter charging a battery, is investigated in detail. The presented approach assumes nonresonant operation (IPT) and is based on the Qi standard specifications. When applied to an RPT system operating exactly at resonance frequency, the reactive part of the system is inherently compensated, and hence the proposed approach shows the same behavior as a synchronous rectifier. However, any deviation from the resonance frequency, caused, e.g., by parameter variations of the passive components, enables a performance increase of the proposed concept over a synchronous rectification approach. An improved control strategy to actively adjust the resistive as well as the reactive part of the equivalent load impedance is introduced in order to optimize the system performance. This approach, applicable to any IPT system, is used to further improve the system efficiency and to extract more power. The presented methodology is based on controlling both the phase-shift of the active rectifier and its output voltage level. This study is an extension to the concept we proposed in [24], where only a simplified system has been investigated and a voltage source at the output of the rectifier is used to set a desired voltage level. In contrast, this paper investigates a complete wireless charging system, including a dc–dc converter to regulate the rectified voltage and a battery as load of the system. The acquired simulations and experimental results show that the proposed concept is capable of achieving significant performance improvements in terms of efficiency and extractable power when compared to prior solutions. The remainder of this paper is organized as follows: In Section II, the theoretical background of the presented methodology is derived and thereafter in Section III the proposed concept is discussed in detail. In Section IV, the applied optimization strategy is introduced and in Section V experimental results

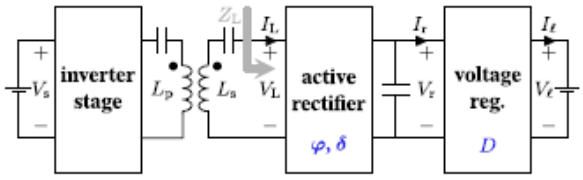

Figure 1. Schematic block diagram of the overall WPT system including an inverter stage driving the primary side resonance circuit, an active rectifier anda dc–dc converter at the secondary side.

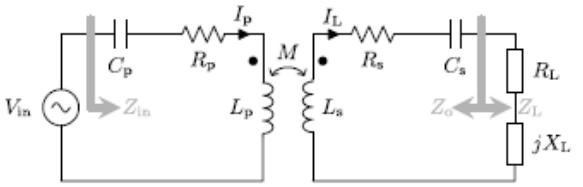

Figure 2. Equivalent circuit model of aseries-series tuned WPT system based on the first harmonic approximation. acquired from the WPT prototype are presented. Finally, in Section VI conclusion

2. WIRELESS CHARGING SYSTEM

ORNL(Oak Ridge National Laboratory) has investigated WPT since 2008, with considerable progress made in the analysis, design, material selection, and performance assessment of stationary and in-motion WPT

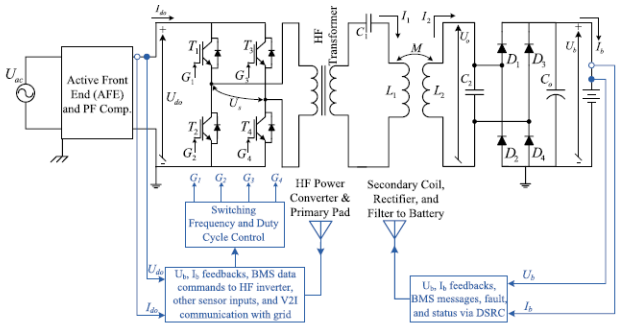

Figure 3 Architecture of primary-side regulation of WPT charging.

Fig4. shows a high-level schematic representation of ORNL's primary-side-regulated WPT system that includes the five power conversion stages. The essential elements of the ORNL's approach are several: 1) an AFE to maintain grid power quality using a boost; 2) an interleaved power factor corrector stage implemented with wide band gap semiconductor devices; 3) a high-voltage power inverter using 1200 V silicon IGBT modules for operation at dc-link voltages from 340 to 800 Vdc; 4) a high-frequency CWT fabricated with low-loss ferrite (MnZn) for which higher flux density FeConano composite is being investigated for future use;5) coupling coils (coupler) fabricated with Litz cable in a planar spiral winding over soft ferrite flux guides; and 6) a loadrectifier using fast recovery diodes over the course of the past three years ORNL researchers have evaluated various tuning means and selected the S–P method as most appropriate for voltage source operation.

The high-frequency rectifier on the secondary side was initially implemented using fast recovery silicon rectifiers of p-i-n structure, then replaced with lower switching loss SiC SBDs that yielded rectifier efficiencies averaging near 99% regardless of operating frequency in the 10–148-kHz WPT spectrum. Specifications for the ORNL wireless charging equipment discussed in this paper are given for single-phase 220 Vac input and a load power of 10 kW, as listed in Table I. The requirement for 10-kW WPT capability comes from the contract that ORNL and partners have with the U.S. Department of Energy (DOE) to develop stationary WPT suitable to

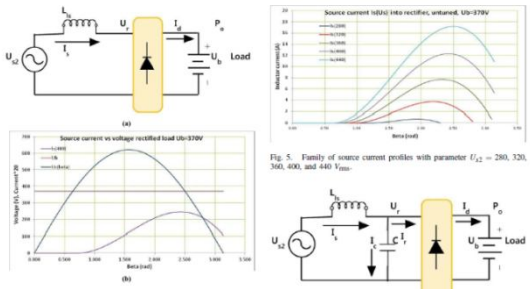

Figure 4. (a) AC source-connected via line inductance to rectify constant voltageload. (b) Waveforms for Us = 400 Vrms,Ub = 370 Vdc, and Is (β),Ls = 122 μH for which Lls = (1 − kz) Lpri = 92.7 μH.

charge either a GM Chevy Volt EREV or Toyota Motor Company RAV4 EV that is standard at 10-kW power charging. Input power requirements from a standard 220 Vac utility connection, and accounting for WPT losses, result in a designbased on 60 A service.

3. Wireless Power Transfer over view

Inductive Coupling: Inductive coupling is based on magnetic field induction that delivers electrical energy between two coils. Figure 5a shows the reference model. Inductive power transfer (IPT) happens when a primary coil of an energy transmitter generates predominantly varying magnetic field across the secondary coil of the energy receiver within the field, generally less than a wavelength. The near-field magnetic power then induces voltage/current across the secondary coil of the energy receiver within the field. This voltage can be used for charging a wireless device or storage system. The operating frequency of inductive coupling is typically in the kilo Hertz range. The secondary coil should be tuned at the operating frequency to enhance charging efficiency . The quality factor is usually designed in small values (e.g., below 10), because the transferred power attenuates quickly for larger quality values . Due to lack of the compensation of high quality factors, the effective charging distance is generally within 20cm. Inductively coupled radio frequency identification (RFID) is an example that pushes the limit to extend the charging distance to tens of centimetres, at the cost of diminished efficiency (e.g., 1-2%) with received power in micro watt range. Despite the limited transmission range, the effective charging power can be very high (e.g., kilowatt level for electric vehicle re-charging).The advantages of magnetic inductive coupling include ease of implementation, convenient operation, high efficiency in close distance (typically less than a coil diameter) and ensured safety. Therefore, it is applicable and popular for mobile devices. Very recently, MIT scientists have announced the invention of a novel wireless charging technology, called MagMIMO , which can charge a wireless device from up to 30cm away. It is claimed that MagMIMO can detect and cast a cone of energy toward a phone, even when the phone is put inside the pocket.

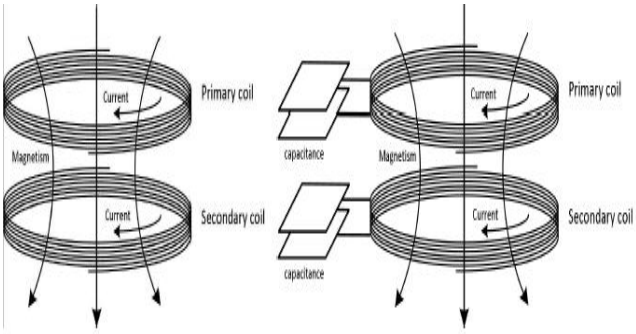

Figure 5. Models of wireless charging systems for inductive coupling and magnetic resonance coupling.

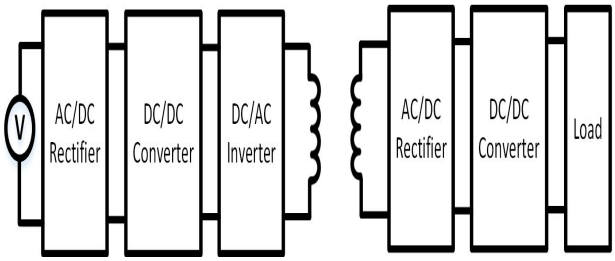

Figure 6. A block diagram of non-radiative wireless charging system.

4.POINT-TO-POINT TRANSMISSION

4.1 Electric and Magnetic Field Strength

With the loop antenna being strongly magnetic compared to other dipole antennas, the reactive near-field is larger than that of a dipole. It is this that makes the loop antenna a good candidate for inductive coupling needed to transfer power to the transponder.

Infinitesimal Small Dipole Phasor Equations :

k = Phase Constant = $\frac{2\pi}{\lambda}$

I_o = Current through the antenna

l = Length of dipole antenna

a = Area of the loop antenna

r = Distance from the center of the antenna

θ = Angle from the z-axis perpendicular to the center of the antenna

$$H_r = H_\theta = E_\phi = 0$$

$$H_\phi = \left[j\omega \frac{kI_o l \sin(\theta)}{4\pi r}\right]\left[1 + \frac{1}{j\omega kr}\right] e^{-j\omega kr} \quad (1)$$

$$E_r = \left[\eta \frac{I_o l \cos(\theta)}{2\pi r^2}\right]\left[1 + \frac{1}{j\omega kr}\right] e^{-j\omega kr} \quad (2)$$

$$E_\theta = \left[j\omega\eta \frac{I_o l \sin(\theta)}{4\pi r}\right]\left[1 + \frac{1}{j\omega kr} - \frac{1}{(kr)^2}\right] e^{-j\omega kr} \quad (3)$$

Reviewing the infinitesimal small dipole field equations the first thing observed is there is only one H-field vector and two E-field vectors. The next item is at θ = 0 degrees only E_r has any magnitude. This shows that with a dipole antenna the E-field is the strongest component strait out from the dipole antenna. Whencomparing the dipole phasor equations 1- 3 to the equations 4 - 6 for a small loop antenna, the primary component shown for the loop antenna is the H-field and the primary component for the dipole is the E-field. Due to the requirement of inductive coupling using a magnetic field the small loop antenna is required.Small Loop Antenna Phasor Equations [17]:

k = Phase Constant $= \frac{2\pi}{\lambda}$

I_o = Current through the antenna

N_t = Number of turns in the loop antenna

a = Area of the loop antenna

r = Distance from the center of the antenna

θ = Angle from the z-axis perpendicular to the center of the antenna

$$E_r = E_\theta = H_\phi = 0$$

$$E_\phi = \left[\eta \frac{(ka)^2 I_0 N_t \sin(\theta)}{4r}\right]\left[1 + \frac{1}{j\omega kr}\right] e^{-j\omega kr} \quad (4)$$

$$H_r = \left[j\omega \frac{ka^2 I_0 N_t \cos(\theta)}{2r^2}\right]\left[1 + \frac{1}{j\omega kr}\right] e^{-j\omega kr} \quad (5)$$

$$H_\theta = \left[-\frac{(ka)^2 I_o N_t \sin(\theta)}{4r}\right]\left[1 + \frac{1}{j\omega kr} - \frac{1}{(kr)^2}\right] e^{-j\omega kr} \quad (6)$$

From the field vector equations for the small loop antenna it is observed that when θ = 0 degrees only H_r is present. Through this experiment the activation distance will be measured off of the z-axis directly out from the loop antenna meaning θ will be 0 degrees. Only the H-field should be seen on this axis.

Before these equations can be plotted in the time domain they must first find the magnitude and phase and then these equations need to be converted to the time domain. To do this first a constant is defined to simply the equation, for H_r is (7).

$$A_r = \frac{a^2 I_0 N_t \cos(\theta)}{2} \quad (7)$$

With (7) defined, (5) can be simplified to:

$$H_r = \left[\frac{A_r}{r^3} + j\frac{\omega A_r k}{r^2}\right] e^{-j\omega kr} \quad (8)$$

Once the vector equation has been simplified, the real and imaginary parts can be isolated and used to find the magnitude and angle equations shown in (9) and (10).

$$|H_r| = \frac{A_r}{r^2}\sqrt{\frac{1}{r^2} + \omega^2 k^2}\,[e^{-j\omega kr + \angle H_r}] \quad (9)$$

$$\angle H_r = \arctan(\omega kr) \quad (10)$$

Now using the phasor to time converting tables the time domain equivalent equations are derived .

$$|h_{r(t)}| = \frac{A_r}{r^2}\sqrt{\frac{1}{r^2} + \omega^2 k^2}\cos(\omega t - \omega kr + \angle h_{r(t)}) \quad (11)$$

$$\angle h_{r(t)} = \arctan(\omega kr) \quad (12)$$

The same derivation to convert the magnitude and angle from the phasor equation is done to the other field vector equations shown in (13 - 16).

$$|h_{\theta(t)}| = \frac{A_\theta}{r}\sqrt{\left(\frac{1}{r^2} - k^2\right)^2 + \frac{k^2}{\omega^2 r}}\cos(\omega t - \omega kr + \angle h_{\theta(t)}) \quad (13)$$

$$\angle h_{\theta(t)} = \arctan\left(\frac{\frac{k}{\omega r}}{\frac{1}{r^2} - k^2}\right) \quad (14)$$

$$|e_{\phi(t)}| = \frac{A_\phi k}{r}\sqrt{k^2 + \frac{1}{\omega^2 r^2}}\cos(\omega t - \omega kr + \angle e_{\phi(t)}) \quad (15)$$

$$\angle e_{\phi(t)} = -\arctan\left(\frac{1}{\omega kr}\right) \quad (16)$$

4.2 MIMO: Let $k^n{}_m$ and $d^n{}_{,m}$ denote coupling co efficiency and distance between the transmit coil n and receive coil m, respectively. In the point-to-point MIMO transmission model, as shown in Figure 9d, the receiver receives the power from each individual transmit coil separately. The crosstalkbetween the transmit coils and receive coils is small . The receive power at the load of the receive coil m 2 {1, . . . ,Nr} from the transmit coil n 2 {1, . . . ,Nt} is given by

$$P_r^{n,m} = P_t^n Q_t^n Q_r^m \eta_t^n \eta_r^m k_{n,m}^2 (d_{n,m}), \quad (17)$$

The total transferred power can be derived as follows

$$P_r = \sum_{n=1}^{N_t}\sum_{m=1}^{N_r} P_r^{n,m}. \quad (18)$$

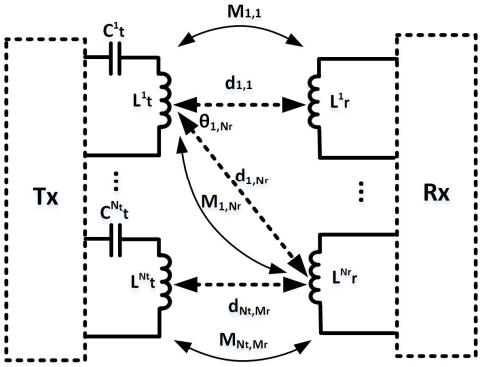

Figure 7. Point-to-point transmission reference models.

5. EXPERIMENTAL RESULTS

5.1Measuring Actual Distance

Once the operating frequency was obtained the next step was measuring the Va and Vr in the circuit to optimize the power being delivered to the antenna. Vr has a common mode of 2.4V which means that a signal carried on this common mode cannot exceed 2 times this value without being in danger of clipping and cause the EM4095 to be unable to decipher the received signal. The documentation from Priority 1 Design states not to exceed 4 Vp-p at Vr to be safe. When using the test setup to measure Vr peak to peak, the external resister (Rs) was replaced with a 100 Ω 20 turn potentiometer. This allowed for a small change in Rs to affect the power being delivered to the antenna. By adjusting Rs to adjust Vr to a value of 4V p-p , the maximum power will be delivered to the antenna for each design. Both the manufactured and second antenna were adjusted to use the same value of Vr to help with the comparison between the 2 antennas.

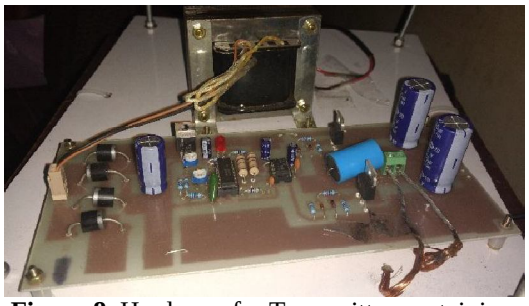

Figure 8. Hardware for Transmitter containing transmission coil beneath**.**

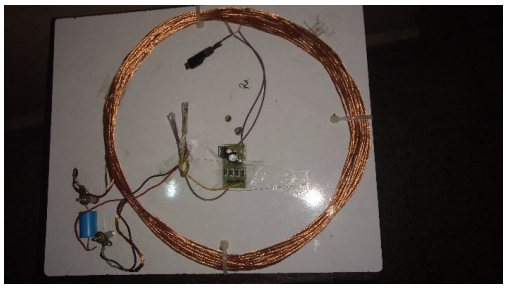

Figure 9. Hardware for Receiver containing receiving coil**.**

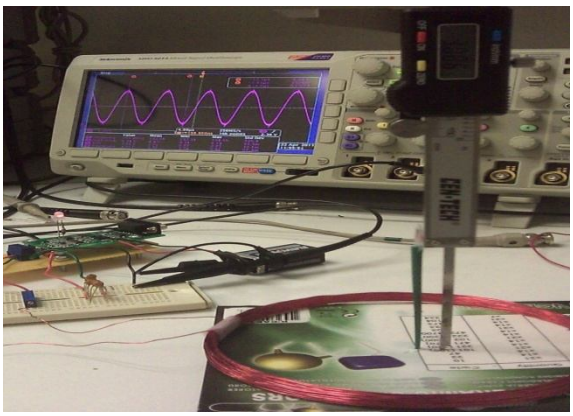

Figure 10.Device Measurement Test Setup

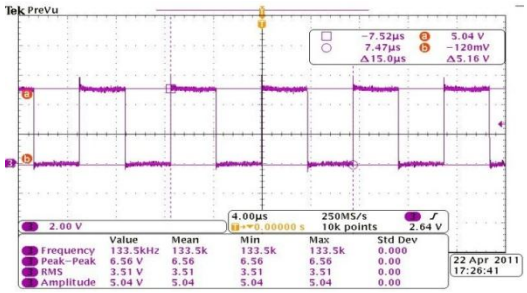

Figure 11. Frequency test point measurement of antenna

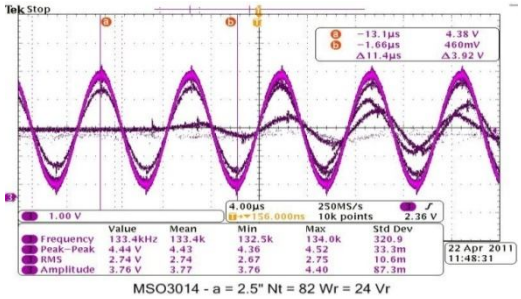

Figure 12. Vr measurement while adjusting Rs

The results can be found in table 1 for all the measured parameters. Note that the first antenna could not exceed 2.32 Vp-p at Vr because without Rs in the circuit the maximum power was already being delievered for this antenna. The reason there was a lack of power pushed through the first antenna is because to obtain the correct operating frequency a tuning capacitor was required in series with the built in capacitor causing a decay of power delivered to the antenna.By adjusting Rs and focusing on Vr due to the fixed capacitor divider built into the circuit, a 4 Vp-p observed on Vr would be the maximum voltage output on Va allowed.

5.2Measuring Activation Distance

Now that the circuit is tuned to the optimum operating effectiveness for each antenna, the read distance is measured. The device has a bi-color LED installed to indicate when a passive LF RFID device is recognized by the microprocessor. This LED does not stay green while a good read is in place, instead it flashes green for 1 pause cycle of 20 ms. This is why the LED is always observed as red in the figures shown.By taking a LF RFID microchip and slowly lowering it in the middle of loop antenna until the indicator flashes green, a activation distance can be read with the micrometer..Table recorded the distance that each antenna obtained a verified read from the FIDRW-E-232.

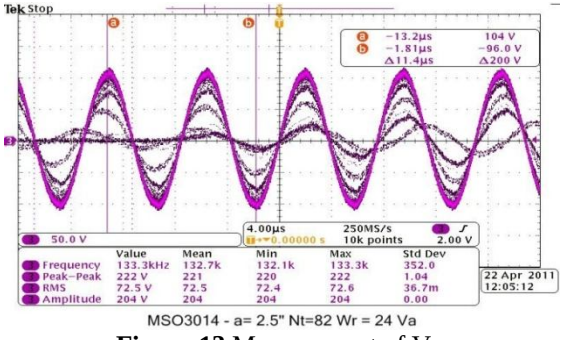

Figure 13. Measurement of Va

Table1: Distance and field measurements

Antenna	Distance (Inch)	H-Field (mV)	E-Field(mV)
Manufactured	2.053	70.4	76
First Antenna	2.564	68.6	33
Second Antenna	3.123	108	42

As the RFID microchip approached the antenna on the z-axis, the validation LED was observed. With the activation and transmission time at 50ms, a slow approach must be made to assure the maximum distance is recorded. As shown in figure 27, a read distance for the second antenna was 3.086 inches. Measuring the distance was done multiple times to identify an average read distance. A the RFID microchip was attached to a small piece of scotch tape and then when the validation light would flash it was attached to the plastic stick. This was done so that accurate measurements could be taken of the read distance.

6. CONCLUSION

Wireless power technology offers the possibility of removing the last remaining cord connections required to replenish portable electronic devices. This promising technology has significantly advanced during the past decades and introduces a large amount of user-friendly applications. In this article, we have presented a comprehensive survey on the paradigm of wireless charging compliant communication networks. Starting from the development history, we have further introduced the fundamental, international standards and network applications of wireless charging in a sequence, followed by the discussion of open issues and envision of future applications. The integration of wireless charging with existing communication networks creates new opportunities as well as challenges for resource allocation.

References

[1] A. RamRakhyani, S. Mirabbasi, and M. Chiao, "Design and optimization of resonance-based efficient wireless power delivery systems for biomedical implants," IEEE Trans. Biomed. Circuits Syst., vol. 5, no. 1, pp. 48–63, Feb. 2011.

[2] M. Zargham and P. Gulak, "Maximum achievable efficiency in near-field coupled power-transfer systems," IEEE Trans. Biomed. Circuits Syst., vol. 6, no. 3, pp. 228–245, Jun. 2012.

[3] R. Wu, W. Li, H. Luo, J. Sin, and C. Yue, "Design and characterization of wireless power links for brain machine interface applications," IEEE Trans. Power Electron., vol. 29, no. 10, pp. 5462–5471, Oct. 2014.

[4] G. Covic and J. Boys, "Modern trends in inductive power transfer for transportation applications," IEEE J. Emerg. Sel. Topics Power Electron., vol. 1, no. 1, pp. 28–41, Mar. 2013.

[5] S. Lukic and Z. Pantic, "Cutting the cord: Static and dynamic inductive wireless charging of electric vehicles," IEEE Electrific. Mag., vol. 1, no. 1, pp. 57–64, Sep. 2013.

[6] S. Choi, J. Huh, W. Lee, and C. Rim, "Asymmetric coil sets for wireless stationary EV chargers with large lateral tolerance by dominant field analysis," IEEE Trans. Power Electron., vol. 29, no. 12, pp. 6406–6420, Dec. 2014.

[7] S. Hui and W. Ho, "A new generation of universal contactless battery charging platform for portable consumer electronic equipment," IEEE Trans. Power Electron., vol. 20, no. 3, pp. 620–627, May 2005.

[8] E. Waffenschmidt, "Wireless power for mobile devices," in Proc. IEEE Int. Telecom. Energy Conf., 2011, pp. 1–9.

[9] Edoardo Charbon, Ranjit Gharpurey, Paolo Miliozzi, Robert G. Meyer, Alberto Sangiovanni- Vincentelli, Substrate Noise – Analysis and Optimization for IC Design, Kluwer Academic Publishers, 2001.

[10] Bruce R. Archambeault, PCB Design for Real- World EMI Control, Kluwer Academic Publishers, 2002.

[11] Liang Dai and Ramesh Harjani, Design of High-Performance CMOS Voltage Controlled Oscillators, Kluwer Academic Publishers, 2002.

[12] E. Ruehli, "Inductance Calculation in a Complex Integrated Circuit Environment," IBM Journal of Research and Development, Vol. 16, No. 5, Sep 1972.

[13] Sequence Design, Inc. "Modeling Skin Effect in Resistive Interconnect," Technology White Paper, 2002.

[14] H. Hasegawa, M. Furukawa, and H. Yanai, "Properties of Microstrip Line on Si-SiO2 System," IEEE Transactions on Microwave Theory and Technology, Vol. 19, Issue 11, Nov 1971.

[15] Andreas Weisshaar, Hai Lan, Amy Luoh, "Accurate Closed-Form Expressions for the Frequency-Dependent Line Parameters of On-Chip Interconnects on Lossy Silicon Substrate," IEEE Transactions on Advanced Packaging, Vol. 25, No. 2, May 2002.

[16] Peter R. Bannister, "Application of Complex Image Theory," Radio Science, Vol. 21, No. 4, Jul 1986.

[17] Harold A. Wheeler, "Transmission Line Properties of A Strip on A Dielectric Sheet on A Plane," IEEE Transactions on Microwave Theory and Technology, Vol. 25, Aug 1977.

AUTHORS

SUJAY RAVI KALE

sujay ravi kale. he received his BE in Electrical, electronics and power from SHREEYASH college of engineering and Technology Aurangabad in 2014. and is Student (M.E) in Electrical Engineering Department MSS's CET, BAMU university, Jalna, Maharastra-431203.

K.chandra obula Reddy, was received B.tech degree from SVCET chitthur (JNTU) in 2009 and M.tech from TOCE Belgaum in 2012. and presently working as Asst.professor, Electrical Engineering Department, MSS's CET, BAMU university, Jalna, Maharastra-431203

ACKNOWLEDGEMENT

I am greatly indebted forever to my guide, to my HOD and all teaching and Non-teaching staff those who support directly and indirectly to complete my project in time. I sincerely thank to my Principal for their continuous encouragement and active interest in my progress that they gave throughout the work.

Iam grateful to Have my Master's degree (EPS) from **Mathshyodhsri shikshan sanstha's** collage of engineering and technology. JALNA, MAHARASTRA.